Eur. J. Mineral.
2011, **23**, 379–390
Published online March 2011

This paper was presented at the EMPG XIII symposium in Toulouse, France (April 2010)

Speciation of As^{III} and As^{V} in hydrothermal fluids by *in situ* X-ray absorption spectroscopy

DENIS TESTEMALE[1,2,*], GLEB S. POKROVSKI[3] and JEAN-LOUIS HAZEMANN[1,2]

[1] Département MCMF, Institut Néel, 25 Avenue des Martyrs, 38042 Grenoble, France
[2] FAME Beamline at ESRF, 6 rue J. Horowitz, 38043 Grenoble, France
*Corresponding author, e-mail: denis.testemale@grenoble.cnrs.fr
[3] Géosciences-Environnement-Toulouse, GET, UMR 5563 of CNRS, University of Toulouse III, 14 Avenue E. Bellin, 31400 Toulouse, France

Abstract: The speciation of arsenic (III) and (V) in aqueous acidic and basic solutions at ambient conditions, and of arsenic (V) in acidic solutions at 270 bars from 30 to 300 °C was investigated using *in situ* X-Ray Absorption Spectroscopy (XAS). Both Extended X-Ray Absorption Fine Structure (EXAFS) analysis and X-Ray Absorption Near Edge Structure (XANES) *ab initio* calculations were used to determine the structure of dominant arsenic species in solution. At ambient conditions, the deprotonation of $As^{III}(OH)_3$ and $As^{V}O(OH)_3$ species with increasing pH is demonstrated by analysis of their XANES signals, in agreement with available arsenious and arsenic acid dissociation constants. In basic conditions, the dominant species is a deprotonated form of the $As(OH)_3$ acid, with a very similar symmetry. The speciation of As^{V} in acidic hydrothermal fluids is dominated by the $As^{V}O(OH)_3$ complex over a wide temperature and pressure range, to at least 300 °C and 300 bars. The first-shell As structure in the $As^{V}O(OH)_3$ species and its deprotonated forms is found to be a distorted tetrahedron, similar to the base AsO_4 unit of $Na_2HAsO_4{\cdot}7H_2O$(s). This work demonstrates new capabilities of XAS coupled with molecular modelling to decipher deprotonation reactions that affect mineral solubilities and chemical elements mobility in aqueous crustal fluids.

Key-words: arsenic speciation, hydrothermal fluid, X-ray absorption spectroscopy, XANES *ab initio* calculations, high-pressure cell.

1. Introduction

Arsenic is a ubiquitous constituent over a wide temperature-pressure (*T-P*) range of natural and industrial environments such as hydrothermal and magmatic metal ore deposits, geothermal fields, mine processing wastes, and many sedimentary rocks and aquifers. The two major biogeochemical features of arsenic, subject of rapidly growing interest, are its toxicity for humans and its close association with economically important metals (Au, Ag, Pt, Cu, Zn, Pb) in ores formed by hydrothermal fluids (*e.g.*, Vaughan, 2006). Accurate knowledge of the identity, stability and molecular structure of dissolved complexes that As forms in aqueous solution is a primary requirement for resolving both ecological and economic issues like remediation of polluted sites, As effect on living organisms, exploration of new metal resources, and efficient and safe ore treatment.

As a result, arsenic mineralogy and aqueous geochemistry has been the subject of many experimental, analytical, thermodynamic and spectroscopic studies over the last 50 years (see Vaughan, 2006; Perfetti *et al.*, 2008 for references). Thanks to these works, we know that at oxidizing surface conditions the main As aqueous species and minerals are arsenates in which As^{+5} is coordinated by four oxygen atoms, similar to phosphates. Like phosphoric acid, arsenic acid exhibits stepwise dissociation in aqueous solution with increasing pH, by forming (hydrogen)arsenate species $AsO(OH)_3^0$, $AsO_2(OH)_2^-$, $AsO_3(OH)^{2-}$ and AsO_4^{3-} (Fig. 1). However, As^{V} becomes unstable with increasing temperature and, at natural hydrothermal conditions, As forms a range of sulphide-arsenide minerals with As valency from −3 to +3, and trivalent neutral hydroxide species, arsenious acid, in aqueous solution (Fig. 1; Pokrovski *et al.*, 2002a, 2002b), similar to other metalloids like B, Si or Ge (*e.g.*, Pokrovski *et al.*, 2005a). The thermodynamic properties of major As-bearing minerals and oxy-hydroxide species obtained from solubility, calorimetric and potentiometric measurements allowed the creation of thermodynamic databases enabling calculations of mineral-fluid-gas equilibria over the range of magmatic-hydrothermal conditions (*e.g.*, Pokrovski *et al.*, 1996, 2005b; Nordstrom & Archer, 2003; Perfetti *et al.*, 2008; Oelkers *et al.*, 2009; references therein).

Although arsenic aqueous speciation in typical low and moderate-temperature natural fluids appears at present to be relatively simple, largely dominated by As^{III} and As^{V} oxy-hydroxide species (Fig. 1) with negligible

0935-1221/11/0023-2104 $ 5.40
DOI: 10.1127/0935-1221/2011/0023-2104

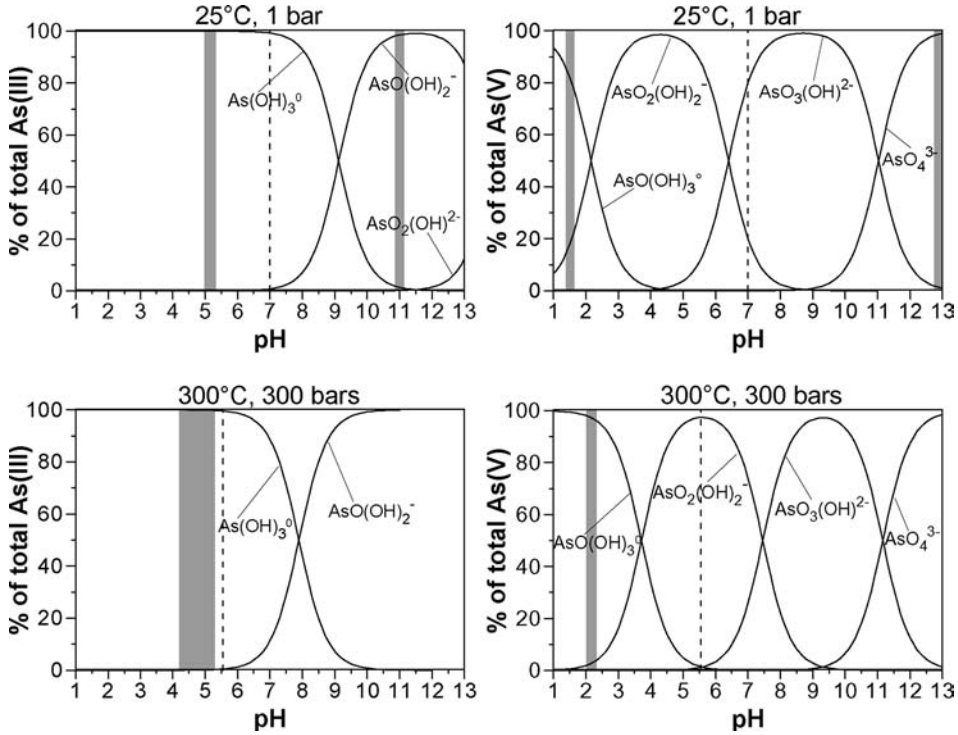

Fig. 1. Distribution of As^{III} (left) and As^{V} (right) hydroxide species in aqueous solution as a function of pH at 25 °C/1 bar and 300 °C/300 bars and an ionic strength of 0.1. The curves were calculated using arsenious and arsenic acids dissociation constants according to Shock *et al.* (1997) for all species except $AsO_2(OH)_2^-$ whose dissociation constant at 25 °C was taken from Nordstrom & Archer (2003). The vertical dashed lines stand for the pH of the neutrality point of water at given temperature and pressure. The vertical grey bars outline the pH ranges of the XAS measurements in this study and those of Pokrovski *et al.* (2002a) and Testemale *et al.* (2004) for As^{III} at elevated temperatures.

contribution in most cases of other As redox states or complexes with other natural ligands (*e.g.*, chloride, sulphide, organic matter), many thermodynamic and structural aspects of As-bearing aqueous complexes remain to be resolved. For example, experimental data on arsenic acid dissociation constants and aqueous As^{V} hydroxide species stabilities are limited to temperatures below 100 °C at atmospheric pressure (*e.g.*, Perfetti *et al.*, 2008), which may potentially introduce significant errors when extrapolating these data to elevated *T-P*. For example, recent findings of arsenate in high *T-P* minerals formed from hydrothermal fluids like skarn garnets (Charnock *et al.*, 2007) or subduction-zone serpentinites (Hattori *et al.*, 2005; Pokrovski & Sanchez-Valle, 2010) contradict the available As^{V}/As^{III} thermodynamics that predicts arsenate to be unstable in such environments (Perfetti *et al.*, 2008). Another issue to be resolved is to better know the speciation of As^{III} in alkaline solutions. If the majority of data agree on the dominant presence of $As(OH)_3$ in acidic to neutral aqueous solution over a wide *T-P* range (Pokrovski *et al.*, 1996) and in hydrothermal and volcanic vapours (Pokrovski *et al.*, 2002a), the stability and structure of its deprotonated forms are less constrained at elevated temperatures. The discrepancies above 250 °C amongst different data sources attain up to 1.5 log unit for the first dissociation constant of $As(OH)_3$ (see discussion by Perfetti *et al.*, 2008), which affects the domain of relative stabilities of $As(OH)_3$ *vs.* $AsO(OH)_2^-$ by 1.5 pH units (Fig. 1), and the solubility of As-bearing minerals by more than one order of magnitude in the near-neutral pH region.

The molecular structures and stoichiometries of aqueous arsenates and arsenites are also insufficiently known, and representations of arsenious acid anion in reference databases vary from AsO_2^- (*e.g.*, Shock *et al.*, 1997) to $As(OH)_4^-$ (Baes & Mesmer, 1976). Such discrepancies affect our understanding of molecular interactions, like solute-solute, solute-solvent and solvent-solvent, which are the fundamental basis of thermodynamic models of crustal fluids (*e.g.*, HKF and density model). They impede accurate predictions of mineral solubilities and solute partitioning coefficients at ''extreme'' conditions, *i.e.*, outside the parameters for a ''classical'' dense aqueous solution, such as low-density fluids and vapours, volatile-rich phases H_2O-CO_2-CH_4 (*i.e.*, co-solvents), or salt-rich brines.

However, most methods (solubility, potentiometry, calorimetry) used to derive thermodynamic properties of aqueous and gaseous species and minerals are insensitive to these structural aspects, which require the use of spectroscopic methods coupled with molecular modelling. Arsenic has largely benefited from such methods in mineral phases, aqueous solution, and silicate melts. Different spectroscopic and theoretical approaches are being used to study As aqueous speciation. The most noticeable ones are Raman (Loehr & Plane, 1968; Gout *et al.*, 1997; Myneni *et al.*, 1998), IR (Myneni *et al.*, 1998;

Pokrovski *et al.*, 1999), and XAS studies (Pokrovski *et al.*, 2002a; Ramirez-Solis *et al.*, 2004; Testemale *et al.*, 2004). Testemale *et al.* (2004) complemented Pokrovski *et al.*'s (2002a) study of As speciation in hydrothermal solutions and vapors, by focusing on the structural changes of the $As(OH)_3$ species with temperature and pressure and relating them to the modifications of the solvent itself. Recently, an X-ray absorption spectroscopy (XAS) study of As in a natural silicate glass (macusanite) showed that As behaviour in hydrous silicate melts is controlled by neutral and/or deprotonated As^{III} hydroxide complexes, similar to those in aqueous fluids (Borisova *et al.*, 2010).

These spectroscopic data were complemented by quantum-chemical calculations of optimized structures and free energies of species. Tossell (1997) applied this method to As^{III} species. He explored the stability of monomeric and oligomeric As^{III} species expected in acid and neutral conditions, and found a good agreement with previous Raman studies (Pokrovski *et al.*, 1996). Myneni *et al.* (1998) used similar methods to explore the structure of the $As^{V}O_4^{3-}$ polyhedron and its interactions with neighbouring molecules in solution. However, this type of calculations still suffers from the complexity of solute-solvent interactions and difficulties of their implementation in computer codes. At the conditions encountered in natural hydrothermal fluids, such as the presence of co-solvents, the existence of a supercritical phase, or very high salinities, such calculations find their limits.

In the last 20 years, XAS proved to be a very useful tool to obtain speciation and molecular structure data, particularly in mineral-fluid systems (*e.g.*, Oelkers *et al.*, 2009). The benefits of this method are manifold. Experimentally, it allows *in situ* measurements of spectra without the need for a quenching of the samples that can be problematic (especially for low-density fluids). Furthermore, all sorts of sample environments set-ups, such as high-pressure and high-temperature cells, can be used. The sensitivity of XAS to the neighbouring shells of the element studied and to its electronic structure makes it a very powerful probe to explore speciation, redox state, ion pairing, and hydration. Within the XAS regime, Extended X-Ray Absorption Fine Structure (EXAFS) formalism is well established and gives access to the radial structure of the element. As a result, its use is widespread (Kelly *et al.*, 2008). X-Ray Absorption Near Edge Structure (XANES) corresponds to the spectral features within ~50 eV above the absorption edge and is more sensitive to electronic and 3-dimensional features of the structure, but at the cost of a more complex formalism that does not have a simple analytical expression. Recently, XANES theoretical developments have grown significantly, enabling a far more quantitative interpretation of spectra. The outcome is the possibility to derive fine speciation information that is not accessible from a more limited EXAFS analysis. In particular, it greatly improves the sensitivity of EXAFS to the coordination parameters such as the number of neighbours, the presence of light atoms like hydrogen, the disorder in the coordination shell, or the nature of the next-nearest coordination sphere. In the case of arsenic, Pokrovski *et al.* (2002a) and Testemale *et al.* (2004) used XAS measurements to obtain As^{III} speciation data in aqueous fluids and vapours to 500 °C/600 bars. The present study extends those works by using similar *in situ* EXAFS measurements to collect speciation data in basic As^{III} and As^{V} solutions and hydrothermal As^{V} solutions and to combine them with quantum-chemistry XANES calculations.

2. Materials and methods

2.1. Experimental samples and conditions

Solid standards were glassy and crystalline cubic (arsenolite) As_2O_3 and $Na_2HAsO_4{\cdot}7H_2O$(s) (Merck, Normapur). They are respectively characteristic of trivalent As^{III}-O_3 and pentavalent As^{V}-O_4 environments that are expected in aqueous solution. They were prepared as fine powder pellets with a thickness optimized for transmission measurements. As^{III} and As^{V} solutions were prepared by dissolution of As_2O_3 and As_2O_5 (Merck, Normapur) in deionized water at 90 °C. Values of pH were adjusted by addition of NaOH. The conditions investigated (concentration, pH, temperature, pressure) are given in Table 1.

The same high-pressure high-temperature cell as in previous studies was used (Soldo *et al.*, 1998; Pokrovski *et al.*, 2002a; Testemale *et al.*, 2004), based on the original design by Tamura and collaborators (1995). It consists of a vessel with Be windows, pressurized with He gas, in which a resistive heater and the sample container are placed. This container is made of polycrystalline sapphire and its design is such that the sample thickness can be optimized for transmission measurements, but it remains constant throughout the whole experiment, *e.g.* during a temperature run. Temperature is regulated by a Eurotherm feedback loop, with a stability within 1 °C. A detailed description of the apparatus was given by Soldo *et al.* (1998) and Pokrovski *et al.* (2002a).

Table 1. Composition of the arsenic aqueous samples, and the conditions of temperature and pressure investigated.

	As concentration ($mol/kg_{solvent}$)	pH at ambient conditions	Temperature (°C)	Pressure (bar)
As_2O_3-H_2O	0.020	5.4	20	1
As_2O_3-H_2O-NaOH	0.020	11.0	20	1
As_2O_5-H_2O	0.200	1.5	30–300	270
As_2O_5-H_2O	0.200	1.5	20	1
As_2O_5-H_2O-NaOH	0.075	13.0	20	1

2.2. X-Ray absorption spectroscopy (XAS) measurements and analysis

XAS spectra of solid and aqueous samples were collected both in transmission and fluorescence mode at the As *K*-edge (11,867 eV) on the spectrometer previously installed on the French CRG beamline BM32 at ESRF. This beamline is equipped with a parabolic Ni-coated mirror and a double-crystal Si(111) monochromator with sagittal focussing, resulting in a spot-size of Full Width Half Maximum (FWHM) $300 \times 200\ \mu m^2$ on the sample. Incident and transmitted signals were collected by Si diodes, and fluorescence counts by a Canberra^{TM} 30 elements solid-state detector.

EXAFS spectra were analysed using the Horae package (Ravel & Newville, 2005) following the classical procedure: normalisation of the spectra, extraction of the oscillations with an evaluation of the baseline, and fitting in the R-space of the structural parameters N (coordination number), *R* (distance to the neighbouring shell) and σ^2 (EXAFS Debye-Waller coefficient, *i.e.*, Mean Square Relative Displacement MSRD parameter). The parameter ΔE_0 which accounts for the misfit in determining the edge energy was also fitted. Effective scattering functions and mean free paths were calculated with FEFF6.0 (Mustre de Leon *et al.*, 1991). Self-absorption effects were estimated using the Booth algorithm (Booth & Bridges, 2005) and were found to be negligible. The asymmetry of the distance distribution was tested by use of the cumulant parameters C_3 and C_4 (Bunker, 1983) but their inclusion did not improve the fits noticeably and they were systematically found to be very small ($<10^{-4}$). Multiple scattering paths were included as well. Two figures of merit were employed to express the goodness-of-fit: the reduced chi-square χ^2 and the *R*-factor. Fitting was done in *R*-space.

The code FDMNES (Joly, 2001) was used to conduct *ab initio* calculations of XANES spectra, both of crystallographic and aqueous structures. It uses full potential calculations within the real space cluster. The final states and resulting absorption cross-sections can be calculated either through the Multiple Scattering (MS) scheme, based on the Muffin Tin (MT) approximated shape of inter-atomic potential, or solving directly the Schrödinger equation in real space using the Finite Difference Method (FDM) which avoids any approximation on the shape of this potential. Details regarding the methodology developed for such calculations are similar to previous studies (Testemale *et al.*, 2004, 2009). In particular, the parameters of convolution of raw calculations are not fitted: they are fixed at 2.14 eV (Lorentzian broadening due to core-hole lifetime at the As *K*-edge, Krause & Oliver, 1979) and 1.6 eV (Gaussian broadening corresponding to the theoretical experimental resolution of the Si(111) monochromator of BM32 beamline). The atoms were kept neutral in all calculations. In our XANES analysis, structural parameters were not fitted. Instead we calculated the XANES spectra of the relevant crystallographic and aqueous structures, as a function of the number and position of protons, H_2O molecules and As-O-As angles, and compared the results to the experimental spectra.

3. Results

3.1. Extended X-ray absorption fine structure (EXAFS)

The results of the EXAFS analysis on As^{III} and As^{V} solid and aqueous compounds are reported in Table 2. The fits done on the structures of As_2O_3 and $Na_2HAsO_4{\cdot}7H_2O$(s) allow us to derive the value of the empirical amplitude reduction factor $S_O{}^2$, by fixing the number of neighbours to the crystallographic value. In both cases very similar values are found, 0.95 for As_2O_3 and 0.96 for $Na_2HAsO_4{\cdot}7H_2O$(s): therefore the value of 0.95 was used in the subsequent fits on the aqueous samples, in which the chemical environment of As is expected to be similar. The average As-O distances found by EXAFS analysis (1.80 Å in As_2O_3 and 1.69 Å in $Na_2HAsO_4{\cdot}7H_2O$(s)) are in agreement with crystallographic values: 1.787 Å in As_2O_3 (Pertlik, 1978) and 1.679 Å in $Na_2HAsO_4{\cdot}7H_2O$(s) (Baur & Kahn, 1970). In the latter, the first shell is distorted and is composed of 4 oxygen atoms at distances between 1.654 and 1.728 Å (Baur & Kahn, 1970). This distortion results in a larger MSRD parameter than in the more symmetric As_2O_3 structure where the three oxygen atoms are at the same distance from the As atom.

Two pH conditions were investigated in As^{III} aqueous solutions, 5.4 and 11.0. The experimental data and fits are plotted in Fig. 2. The speciation of As^{III} in aqueous solution is known (see Fig. 1 and Pokrovski *et al.*, 2002a): the species $As(OH)_3$ is the dominant As complex below pH 9, and its deprotonated anions at higher pH. The EXAFS results obtained here at acidic pH are in agreement with this speciation, yielding three oxygen neighbours at 1.79 Å, but no information about the presence of H atoms to which EXAFS is very little sensitive.

Fits of EXAFS spectra of acidic and basic samples yield distinct structural parameters. The amplitude parameters *N* and σ^2 change from acid to basic conditions: from 3.0 to 3.6 oxygen atoms around As, and from 2.3 to 7.5×10^{-3} $Å^2$ respectively. This may indicate a possible change of coordination around the As atom, from three-fold to four-fold (or a mixture of both). But if this was the case, the As-O distance would also be impacted whereas the distance remains identical at 1.79 Å $\pm$ 0.01. Furthermore, the EXAFS amplitude parameters are highly correlated, especially the number of neighbours N and the MSRD parameter σ^2. The consequence is visible in Table 2 where two sets of fitting parameters are reported for the basic As^{III} solutions: in the second, the number of neighbours was fixed at 3.0 and the resulting σ^2 parameter changes only slightly from 7.5×10^{-3} to 6.1×10^{-3} $Å^2$, at a very reduced cost in fit quality (*R* and χ^2 increase from 0.017 to 0.023, and from 39 to 44, respectively). These EXAFS observations thus seem to indicate a similar structural environment of As^{III} in a wide range of pH.

Recently Ramirez-Solis *et al.* (2004) proposed a structure with two As-O distances for arsenious acid in basic solution (one oxygen atom at 1.69 Å and two oxygen atoms at 1.82 Å). This possibility has been tested (not shown) but could never converge to a stable set of parameters and

Table 2. Results of the EXAFS analysis on crystallographic and aqueous samples. For all aqueous samples, the amplitude parameter S_O^2 is set at 0.95, based on the fit done on glassy As_2O_3.

Sample	*T*/*P*	*N*	*R* (Å)	MSRD σ^2 (Å$^2 \times 10^{-3}$)	ΔE_0 (eV)	R/χ^2	Measurement	k (Å^{-1}) and R (Å) ranges
Glassy As_2O_3	amb.	3[a]	1.80 ± 0.010	3.2 ± 0.9	12.0 ± 2.2	0.028/146	Trans	[2.6–15.3] [1.0–2.2]
Cubic As_2O_3	amb.	3[a]	1.80 ± 0.010	3.1 ± 0.7	11.5 ± 2.0	0.019/135	Trans	[2.6–15.3] [1.0–2.2]
Aqueous As^{III} 0.02 m pH = 5.4	amb.	3.0 ± 0.1	1.79 ± 0.010	2.3 ± 0.3	13.5 ± 0.8	0.003/10	Fluo	[4.0–14.0] [1.0–2.6]
Aqueous As^{III} 0.02 m pH = 11.0	amb.	3.6 ± 0.5	1.79 ± 0.010	7.5 ± 1.3	12.7 ± 2.1	0.017/39	Fluo	[4.0–12.4] [1.0–2.6]
Aqueous As^{III} 0.02 m pH = 11.0	amb.	Fixed 3	1.79 ± 0.010	6.1 ± 0.7	13.7 ± 2.2	0.023/44	Fluo	[4.0–12.4] [1.0–2.6]
Cryst. $Na_2HAso_4{\cdot}7H_2O$(s)	amb.	4[b]	1.69 ± 0.020	4.7 ± 1.9	4.8 ± 3.6	0.033/138	Trans	[2.6–10.8] [0.8–2.4]
Aqueous As^{V} 0.2 m pH = 1.5	amb.	4.3 ± 0.2	1.70 ± 0.003	3.7 ± 0.3	3.4 ± 1.2	0.003/63	Trans	[4.1–15.6] [0.8–2.2]
Aqueous As^{V} 0.075 m pH = 13	amb.	4.5 ± 0.3	1.70 ± 0.030	2.4 ± 0.3	6.0 ± 1.3	0.004/158	Trans	[4.1–15.6] [0.8–2.2]
Aqueous As^{V} 0.2 m	30 °C/270 bars	4.1 ± 0.7	1.69 ± 0.010	3.1 ± 1.2	2.9 ± 3.5	0.021/104	Trans	[4.1–12.2] [0.8–2.2]
Aqueous As^{V} 0.2 m	100 °C/270 bars	4.1 ± 0.7	1.70 ± 0.010	3.3 ± 1.3	3.5 ± 3.4	0.021/124	Trans	[4.1–12.2] [0.8–2.2]
Aqueous As^{V}0.2 m	150 °C/270 bars	4.1 ± 0.7	1.70 ± 0.010	3.7 ± 1.3	3.6 ± 3.4	0.021/115	Trans	[4.1–12.2] [0.8–2.2]
Aqueous As^{V} 0.2 m	200 °C/270 bars	4.1 ± 0.7	1.70 ± 0.010	3.8 ± 1.3	3.1 ± 3.4	0.021/112	Trans	[4.1–12.2] [0.8–2.2]
Aqueous As^{V} 0.2 m	250 °C/270 bars	3.9 ± 0.7	1.70 ± 0.010	3.6 ± 1.3	2.7 ± 3.5	0.022/92	Trans	[4.1–12.2] [0.8–2.2]
Aqueous As^{V} 0.2 m	300 °C/270 bars	4.0 ± 0.8	1.70 ± 0.010	4.4 ± 1.5	1.8 ± 3.7	0.025/114	Trans	[4.1–12.2] [0.8–2.2]

[a]The number of neighbours is fixed at 3 and the amplitude parameter S_O^2 is fitted and found equal to 0.95.
[b]The number of neighbours is fixed at 4 and the amplitude parameter S_O^2 is fitted and found equal to 0.96.

always resulted in large uncertainties (uncertainties are not given by Ramirez-Solis *et al.*, 2004). This is due to the limited exploitable spectral range and the increased number of variables needed for such a multi-shell fit. Hence, this structure cannot be ruled out at this stage, but any firm conclusion regarding its existence based only on EXAFS analysis appears doubtful.

Two pH conditions were also investigated in As^{V} aqueous solutions, 1.5 and 13.0. The EXAFS fits (Table 2) indicate that the structures in both solutions are identical within uncertainties ($N = 4.3$ and $R = 1.70$ Å). The only difference is the average value of MSRD parameter that decreases from 3.7 to 2.4 $\times$ 10^{-3} Å^2 with increasing pH. This could be an indication of a more symmetrical (*i.e.*, less distorted) structure in basic conditions where all oxygen atoms are deprotonated in the AsO_4^{3-} species (Fig. 1). Borisova *et al.* (2010) reported the same MSRD evolution for As^{V} basic solutions, although they obtained a larger number of oxygen neighbours (5 ± 1). The speciation of aqueous As^{V} at hydrothermal conditions as a function of temperature has been examined at acidic pH. The results are reported in Table 2 and experimental spectra and fits are plotted in Fig. 3 for the lowest and highest temperatures investigated, 30 °C/270 bars and 300 °C/270 bars. The EXAFS parameters are similar at all temperatures: four oxygen neighbours are found around As, at a distance of 1.70 Å. The only noticeable evolution is in the disorder MSRD parameter which increases from 3.1 to 4.4 $\times$ 10^{-3} Å^2 from 30 to 300 °C. This four-fold coordination most likely corresponds to the species $AsO(OH)_3$, similarly to As^{III} aqueous speciation, dominated by $As(OH)_3$ from ambient to high-temperature conditions (up to 500 °C, Pokrovski *et al.*, 2002a; Testemale *et al.*, 2004). The same slight increase of the disorder parameter σ^2 was observed: for $As(OH)_3$ species, Testemale *et al.* (2004) found an increase of σ^2 from 1.2 to ~2.0 $\times$ 10^{-3} between 30 and 300 °C. Our results are also in agreement with a recent XAS study conducted on As-rich fluid-inclusions (James-Smith *et al.*, 2010): they reported 4.3 oxygen neighbours at 1.70 Å for an aqueous solution of sodium arsenate $HAs^{V}O_4^{2-}$ (pH ~7) at ambient conditions.

Although EXAFS analysis provides useful quantitative information on the general coordination environment of As, it is poorly sensitive to the presence of protons and thus does not allow unambiguous distinction between different protonated species of As in solution. XANES spectra may provide such information; they are discussed in the following section.

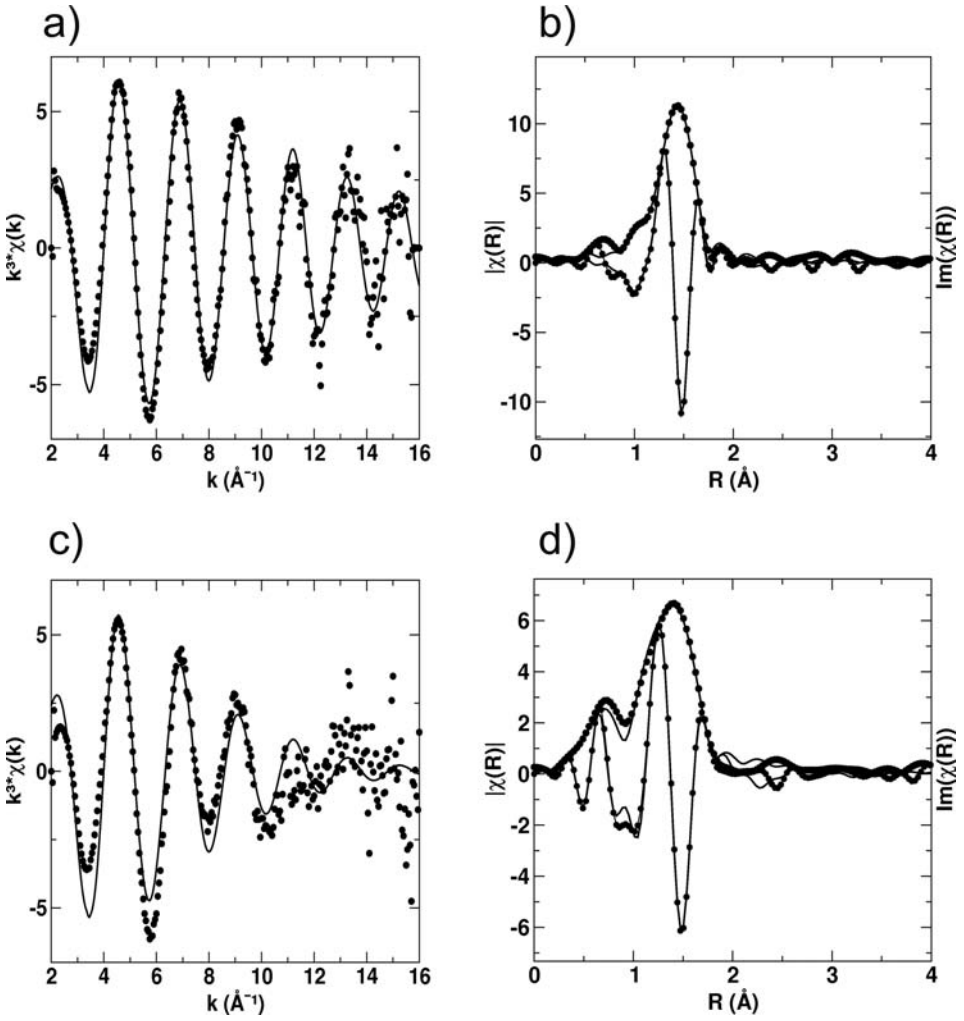

Fig. 2. (a) and (b) EXAFS k^3-weighted oscillations and amplitude and imaginary parts of the Fourier transforms (not corrected for phase-shift) of the 0.02 m As^{III} solution at pH 5.4, ambient conditions; (c) and (d) EXAFS k^3-weighted oscillations and amplitude and imaginary parts of Fourier transforms (not corrected for phase-shift) of the 0.02 m As^{III} solution at pH 11.0, ambient conditions. The feature below 1 Å in panel (d) is a residual of an imperfect background subtraction due to the low signal-to-noise ratio of the data, caused by strong absorption of the fluorescence signal by Na^+ ions in this alkaline solution.

3.2. X-ray absorption near edge structure (XANES)

XANES calculations were done on both solid standards and aqueous structures. The former are known, and in this case the calculations are useful to probe the capability of the code to reproduce XANES features characteristic of their stereochemistry; electronic and other code-specific parameters are optimized during this step. The structures of aqueous complexes are unknown, or at least hypothetical, and the objective is to derive as much structural information as possible through comparison of experimental and calculated XANES spectra. The choice of the crystallographic standards was made according to the coordination of As atoms in As_2O_3 and $Na_2HAsO_4{\cdot}7H_2O$(s), which is respectively three-coordinated As-O_3 and tetra-coordinated As-O_4 (see Fig. 4). Thus the accurate comparison of their spectra with those of aqueous samples helps to constrain the XANES models below.

The experimental and calculated spectra for cubic As_2O_3 (Pertlik, 1978) are reported in Fig. 5. The coordination environment of As in this compound is not symmetrical: one side is occupied by the three nearest oxygen atoms shared within the As_4O_6 cluster, the other side is an empty space with the nearest neighbours lying more than 3 Å away (Fig. 4). This made the use of the FDM method necessary in FDMNES calculations, even if they are much more computer intensive. The reason stems from the approximated Muffin-Tin shape of the potential that was shown to result in incorrect calculations, especially in the energy region (∼20 eV) of the absorption edge, in situations where the local environment is not dense and symmetrical (Joly, 2001). The influence of the radius of calculation, *i.e.* the distance within which atoms are included in the calculation, was evaluated and is reported in Fig. 5. The three values of 2.0, 3.5 and 4.5 Å correspond to the inclusion, within the sphere of calculation, of respectively the AsO_3 group alone, the As_4O_6 group alone, and As_4O_6 with several As and O atoms of the neighbouring As_4O_6 groups. As expected, the best agreement with the

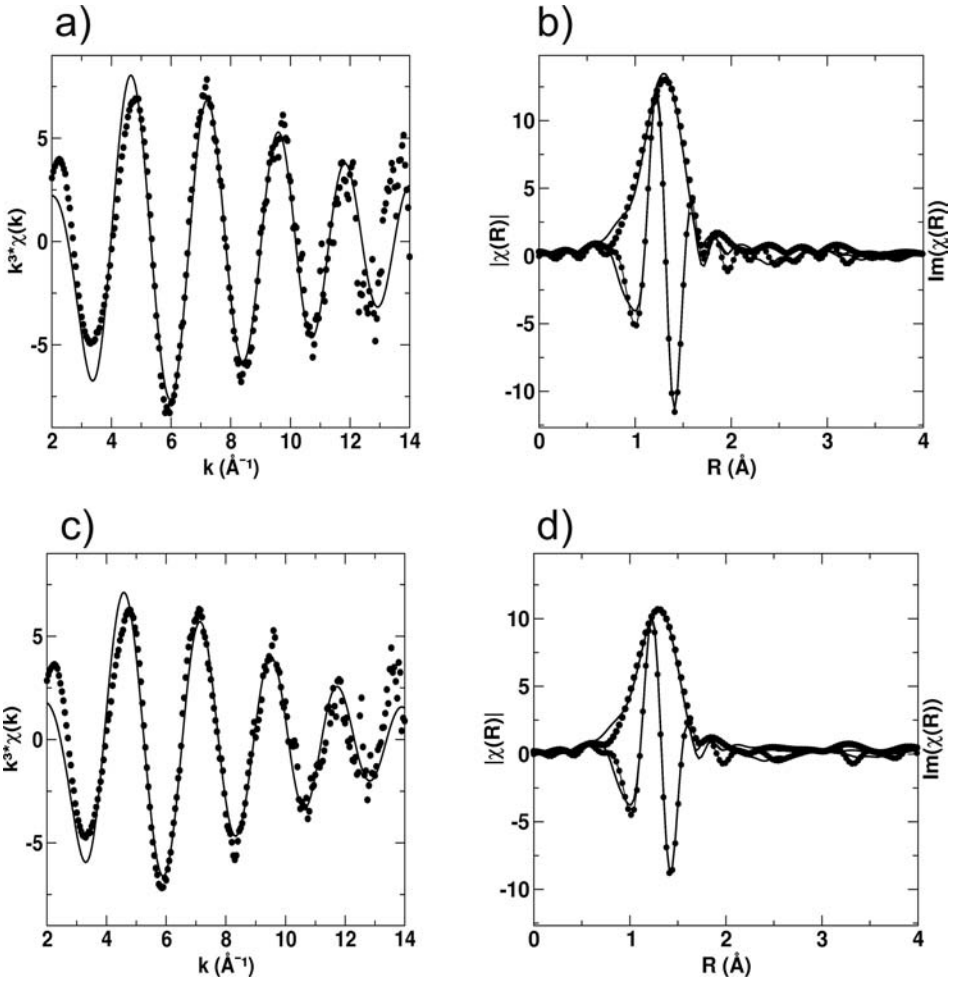

Fig. 3. (a) and (b) EXAFS k^3-weighted oscillations and amplitude and imaginary parts of the Fourier transforms (not corrected for phase-shift) of the 0.2 m As^V solution, pH = 1.5, at 30 °C/270 bars; (c) and (d) EXAFS k^3-weighted oscillations and amplitude and imaginary parts of Fourier transform (not corrected for phase-shift) of the 0.2 m As^V solution, pH = 1.5, at 300 °C/270 bars.

experimental spectra of cubic and glassy As_2O_3 is obtained with the largest radius. It must be noted however that with only the As_4O_6 groups (R = 3.5 Å), the agreement is satisfactory but the features within the first 20 eV above the absorption edge can only be reproduced correctly by taking into consideration the neighbouring atoms further away (R = 4.5 Å). Finally, with only the AsO_3 groups, the agreement is obtained above 11,900 eV, *i.e.* almost in the EXAFS region where the first distance As-O yields the dominant contribution to the EXAFS oscillations. In Fig. 5, the slight shift towards higher energy of the AsO_3 calculated spectrum likely stems from the nature of the As-O bond: the electron density is more localized, *i.e.* As atoms are locally more oxidized, than in As-O-As or As-O-H bonds where electron density is spread towards neighbouring As and H atoms.

The speciation of As^{III} in aqueous acid to slightly basic conditions is dominated by $As(OH)_3$ (Pokrovski *et al.*, 2002a), which has a symmetry very similar to the AsO_3 unit present in As_2O_3. This is the reason why, in Fig. 5, the agreement is good between the overall shape of the experimental spectrum obtained in near neutral conditions and the shape of the calculated spectrum within 2 Å, where As-O-As bonds are not taken into account. It can be seen in Fig. 6 that the influence of pH is very weak and the main differences are localized between 11,870 and 11,900 eV. The overall resemblance of the two spectra collected at different pH is a good indication that the structure of As^{III} species in basic conditions is similar to $As(OH)_3$ dominant in acid conditions. The small difference observed may be due to (1) a modification of the number and position of hydrogen atoms linked to the three oxygen atoms; this possibility is in agreement with the basic conditions that promote the deprotonation and the appearance of charged species $AsO_3H_n^{(n-3)}$; (2) a modification of the second shell, driven by interactions between the charged species $AsO_3H_n^{(n-3)}$, the surrounding water molecules and Na^+ cations. To illustrate the effect of H atoms in point (1), we calculated XANES spectra of four possible aqueous species, corresponding to the stepwise removal of hydrogen atoms: $As(OH)_3$, $AsO(OH)_2$, $AsO_2(OH)$ and AsO_3. The geometry of the AsO_3 entity in these species is adapted from Testemale *et al.* (2004), with the structure of $As(OH)_3$

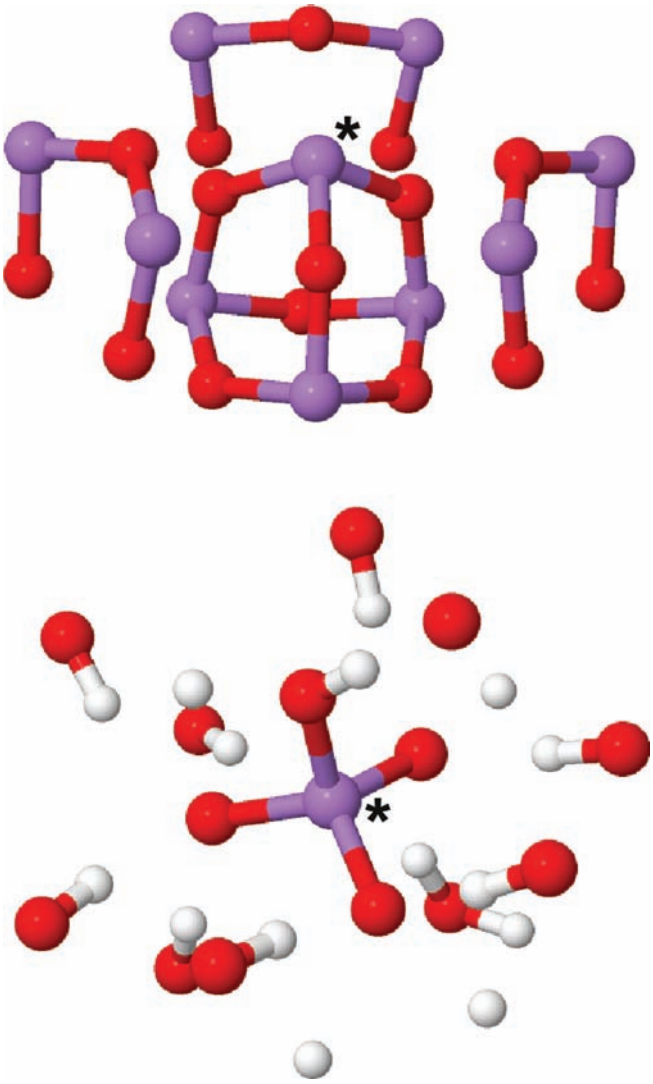

Fig. 4. Top: Balls and sticks 3D view of the cubic As_2O_3 structure (mauve = As, red = O) with the characteristic As_4O_6 units (Pertlik, 1978); the atoms shown are within 4.5 Å of the central As atom (marked with a star). Bottom: Balls and sticks 3D view of the $Na_2HAsO_4{\cdot}7H_2O$(s) structure (mauve = As, red = O, white = H) with the characteristic AsO_3OH unit (Baur & Kahn, 1970); the atoms shown are within 4 Å of the central As atom (marked with a star). These two radii are the largest ones used for the XANES calculations (see text). Colours refer to the online version.

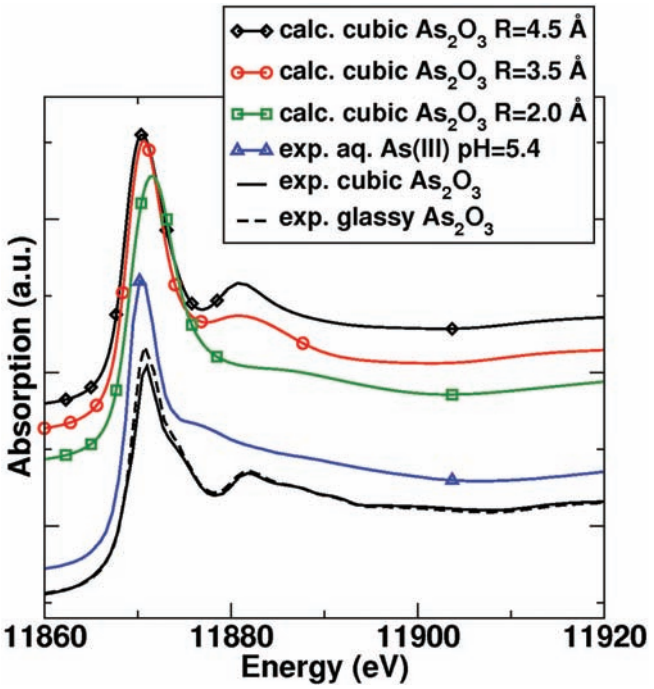

Fig. 5. Experimental and calculated XANES spectra of As^{III} solid and aqueous (pH = 5.4) samples. *R* is the radius of the spherical volume of calculations. The spectra are offset vertically for clarity. Colour online.

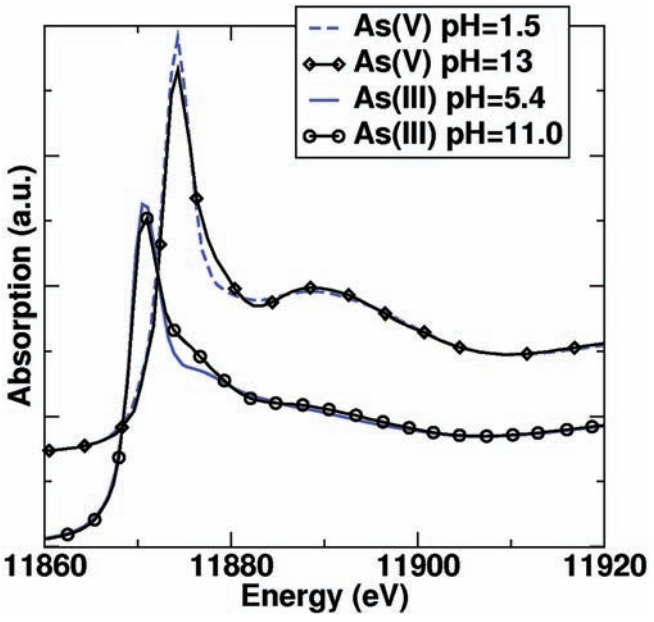

Fig. 6. Experimental XANES spectra of As^{III} and As^{V} solutions at acid and basic conditions. Colour online.

having a C_{3V} symmetry, As-O distance of 1.77 Å, O-As-O angles of 98° and As-O-H angles of 120°. The atoms are kept neutral. The resulting spectra are plotted in Fig. 7. The purpose here is not to determine which one of those spectra is closest to the experimental one, but to illustrate the impact of deprotonation in the XANES calculations. Besides, it could be argued that such a deprotonation would be accompanied by a slight distortion of the AsO_3 structure, both in terms of inter-atomic distances and angles, but it is not taken into account here. In Fig. 7, it can be seen that the energy range over which H atoms have an influence is limited to the white line, *i.e.* between ~11,865 and 11,880 eV. This impact of hydrogen atoms and also of a second shell of water molecules on XANES spectra had already been investigated in the case of Ni^{2+} hydration by D'Angelo *et al.* (2006), by placing the hydrogen atoms in the so-called ''dipole configuration'' and using the position of the second shell of water molecules derived from molecular dynamics simulations. Testemale *et al.* (2009) did a similar investigation for Fe^{2+} hydration,

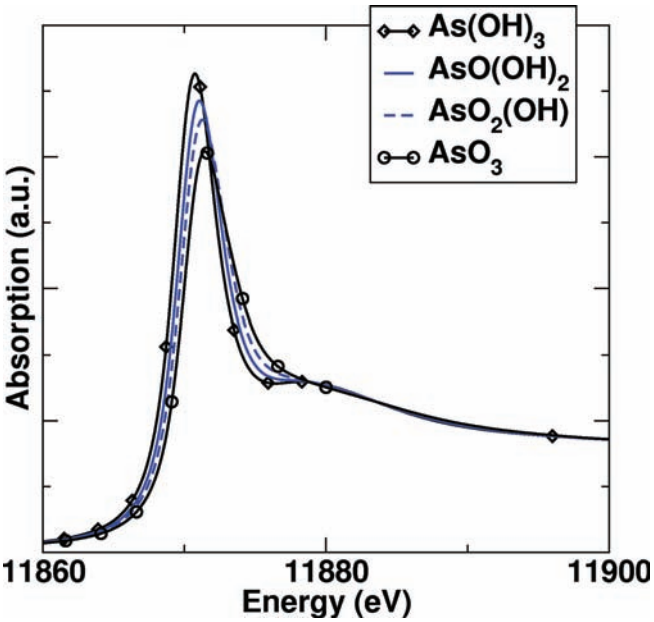

Fig. 7. Calculated XANES spectra of AsO_3 clusters with varying the number of hydrogen atoms. Colour online.

placing the H atoms in the same ''dipole configuration'' but positioning twelve second-shell oxygen atoms in a very symmetric, and likely unrealistic, position to enhance artificially the effect of second-shell water molecules and thus better identify their effect of XANES spectra. The conclusion that we draw in the present case of arsenious acid species is identical to what was found in those previous studies: the presence of hydrogen atoms (and second-shell water molecules) modifies slightly the XANES features within the first 20 eV above the absorption edge. This is precisely the energy region where differences in the XANES spectra of the As^{III} samples at two different pH show up (Fig. 6). Furthermore, the trend observed in the calculations with an increase of the number of H atoms (Fig. 7, increase of the intensity of the white line and formation of a ''dip'' at its base) agrees with the experimental observations as a function of pH.

This study confirms that deprotonated arsenious acid species are dominant at basic conditions, in perfect agreement with the well known As^{III} speciation at ambient conditions as a function of pH (Fig. 1). The great sensitivity of XANES to the species symmetry and to the presence of protons demonstrated in this study opens new possibilities of exploring, in the near future by this original method, As^{III} acid-base equilibria at elevated *T-P*, where they are a subject of much greater discrepancies (see ''Introduction'' and Perfetti *et al.*, 2008).

Following the idea mentioned above that a distortion of the molecule is also possible, XANES calculations on the structure that Ramirez-Solis *et al.* (2004) proposed for the As^{III} species in basic pH solutions have also been done (the results are not shown here). However it could not be investigated in details as we have no clue of the possible three-dimensional symmetry. The XANES spectra of a distorted trigonal cluster AsO_3 with two distances (twice 1.82 Å and once 1.69 Å) and of a symmetric AsO_3 cluster with three equal As-O distances (1.77 Å) are very similar in the region of the absorption edge, *i.e.* the first 20 eV. As in the case of the EXAFS analysis, this structure cannot be ruled out based on such a rough XANES analysis, but there are indications that changes in H atoms and/or the second shell are better candidates to explain the experimental XANES spectral changes with pH.

Two different radii (2.5 and 4 Å) have been used in XANES calculations of $Na_2HAsO_4{\cdot}7H_2O$(s) (Baur & Kahn, 1970), corresponding to the inclusion of the AsO_3OH unit and additional second-shell water molecules (see the 3D view of the structure in Fig. 4). The results are plotted in Fig. 8. It can be seen that the calculations with the AsO_3OH unit (radius 2.5 Å) match well the position and amplitude of the main features of the experimental spectrum (except for the white line which is too high in the calculations). In the case of As^{III} structures, a larger radius of calculation was needed to reach the same agreement. The reason is the more compact tetrahedral geometry of the $As^{V}O_4$ units where the As atoms are more screened from the environment than they are in pyramidal $As^{III}O_3$ units. The same observation was done for XANES calculations in two types of Cu structures, linear CuO_2 unit and tetrahedral $CuCl_4$ (Brugger *et al.*, 2007): in the latter the Cl atoms screen the Cu atom from the environment and limit the influence of second and more distant shells. In the case of $Na_2HAsO_4{\cdot}7H_2O$(s), extending the cluster to 4 Å improves the agreement with the experimental features, especially the oscillation at 11,885 eV, but the height of the white line is still poorly reproduced. A larger radius of calculation is probably needed, that includes more than the water molecules: the nearest Na atoms are beyond 4.5 Å and the nearest As atoms beyond 6 Å. But even with a

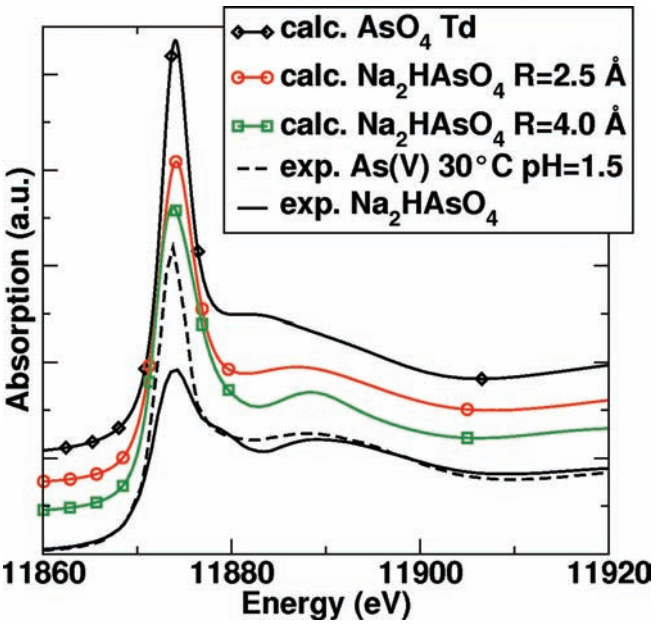

Fig. 8. Experimental and calculated XANES spectra of As^{V} solid and aqueous samples. The spectra are shifted vertically for clarity. Colour online.

radius limited to 4 Å, calculations are very costly because of the lack of symmetry of the structure.

In Fig. 8, the experimental spectrum of the aqueous As^V sample at 30 °C/pH = 1.5 is also reported. Two points must be noted here: (1) the features of this spectrum and their positions are similar to those of $Na_2HAsO_4{\cdot}7H_2O$(s), and (2) the amplitude of the white line is larger for the aqueous sample. These are qualitative indicators of the similarity between the structure of aqueous As^V species and the characteristic AsO_3OH unit of $Na_2HAsO_4{\cdot}7H_2O$(s), but with a much larger disorder in the shells beyond the first one. This is confirmed by the calculations: the agreement between the experimental aqueous As^V XANES spectrum and the calculated spectrum of AsO_3OH (*i.e.*, within 2.5 Å) is very good for the amplitude of the white line and the shape and position of the features. Note that the agreement is poor in case of a regular tetrahedron AsO_4, with the As-O distance 1.69 Å derived from EXAFS fits (see Table 2). It has been verified that this disagreement is not due to the absence of a hydrogen atom. As it can be seen in Fig. 1, thermodynamic data indicate that the dominant species at 25 °C/300 bars in acidic conditions is $AsO(OH)_3$. From this and the XANES calculations, we conclude that the speciation of As^V in acidic solution at 30 °C is dominated by the $AsO(OH)_3$ tetrahedral species, distorted similarly to the AsO_3OH unit in $Na_2HAsO_4{\cdot}7H_2O$(s). In alkaline solution, the species AsO_4^{3-} is thermodynamically stable (Fig. 1). The corresponding XANES spectra are plotted in Fig. 6. It can be seen that the differences between acidic and basic conditions are similar to those of As^{III} solutions: for lower pH, the intensity of the white line is higher and one can observe the formation of a ''dip'' at its base at about 11,880 eV. XANES calculations (not shown here) confirmed that the effect of removing H atoms from the species $AsO(OH)_3$ is the same as in the case of $As(OH)_3$ (Fig. 7). Finally, by observing Fig. 6 and 8, it appears that the calculated spectrum of a perfectly tetrahedral AsO_4 species matches neither the XANES spectrum of $AsO(OH)_3$ nor that of AsO_4^{3-}, and that the distorted AsO_4 structure characteristic of $Na_2HAsO_4{\cdot}7H_2O$(s) is a better candidate. This distortion is supported by the recent experimental (Raman and IR) and computational study of the structure of the AsO_4^{3-} polyhedron showing that this polyhedron was strongly distorted when protonated, solvated by water molecules or bound to metal cations (Myneni *et al.*, 1998).

The evolution of As^V speciation with temperature is illustrated in Fig. 9. It can be seen that the changes of the XANES spectra are very weak: there is neither appearance of new features, nor shift of the existing ones or changes in the white line. The only modifications visible at the minimum around 11,882 eV (feature B) and, to a smaller degree, the minimum at 11,910 eV (feature C) are interpreted as a global reduction of the amplitude of oscillations due to increasing temperature leading to thermal disorder. It is equivalent to the dampening of EXAFS oscillations by the MSRD disorder term. As already demonstrated above, this energy region is also the one where changes in hydrogen configurations and second-shell modifications (such as a disordering due to temperature rise) may impact the XANES spectra. This impact is smaller in the case of As^V structures due to the screening of the As atoms by the tetrahedral oxygen shell (see above). Hence, the nature and the very small amplitude of the changes observed in Fig. 9 indicate that thermal disorder is the main effect. The resulting ''stability'' of the AsO_3OH unit is in agreement with EXAFS results where only a small increase of the MSRD disorder parameter was observed, most likely related to the increase of temperature.

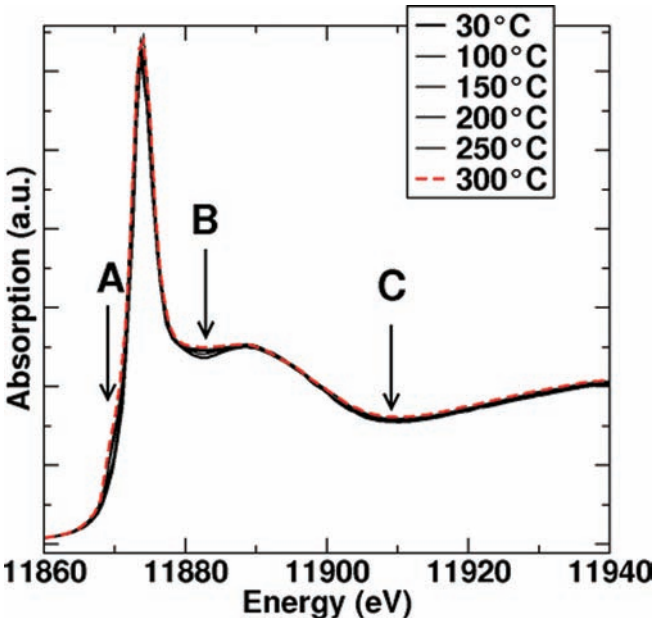

Fig. 9. Experimental XANES spectra of As^V aqueous samples at 270 bars, from 30 to 300 °C. Arrows A, B and C indicate spectral changes with temperature (see text). Colour online.

In Fig. 9, it can also be noted the appearance of a small shoulder on the low energy side of the white line, slightly growing with temperature (feature A). Its energy position corresponds to the white line in As^{III} spectra. A linear combination fit was done on the As^V samples, with the tool provided in Athena software (Ravel & Newville, 2005), using As^{III} and As^V solutions at 30 °C as standards: the fit yielded a maximum As^{III} fraction of 12 mol% in the sample (this proportion was obtained at 300 °C and is smaller for lower temperatures). The origin of this reduction of As^V is still unclear: this reduction may be due to beam-induced artefacts, typical for redox sensitive elements, especially at high temperatures.

4. Discussion

4.1. Speciation

The results of this study can be first interpreted in terms of arsenic speciation. Complementary EXAFS and XANES analyses confirm that the As^{III} species that predominate in basic conditions are deprotonated forms of the $As(OH)_3$ arsenious acid (Fig. 1). EXAFS analysis points to a structure with three oxygen neighbours around the arsenic atom,

like in acid conditions. This structure is undoubtedly confirmed by the XANES signature, very similar to acid conditions where $As(OH)_3$ dominates, and *ab initio* XANES calculations indicating that the differences between the spectra in acid and basic conditions are compatible with the deprotonation of $As(OH)_3$. These spectroscopic results are in good agreement with thermodynamic data on As^{III} speciation: at these pH and temperature conditions, $AsO(OH)_2^-$ is the dominant As form (Fig. 1).

In the case of As^{V} solutions, the EXAFS and XANES analyses both converge towards the predominance of a distorted tetrahedral AsO_4 structure, similar to the distorted moiety in the structure of $Na_2HAsO_4{\cdot}7H_2O$(s) (Fig. 4). At ambient temperature, this is a confirmation of the existence of the $AsO(OH)_3$ species in solution (Fig. 1). In basic conditions, the deprotonation of this species is observed from the XANES spectra (Fig. 6) that are interpreted by means of the XANES *ab initio* calculations. They also confirm the existing dissociation constants of arsenic acid, but an additional information retrieved from our analysis is the persistence of a distorted tetrahedral structure for the AsO_4^{3-} species. This sensitivity of the spectra to the protonation of aqueous species is a very promising aspect of our study. Indeed, it can be a powerful tool to explore, using XANES modelling, acid-base equilibria in challenging experimental conditions where only *in situ* XAS measurements are possible.

At higher temperatures, up to 300 °C, we interpret the very weak changes in the XANES spectra as the manifestation of thermal disorder, in agreement with the small increase of the MSRD EXAFS parameter observed with temperature. Consequently, as in the case of As^{III} speciation under hydrothermal conditions (Pokrovski *et al.*, 2002a; Testemale *et al.*, 2004), the speciation of As^{V} does not change with temperature and remains dominated by $AsO(OH)_3$, also in agreement with available thermodynamic data (see Fig. 1). It must be noted, however, that we observed a small reduction of less than 12 % of As^{V} to As^{III} at the highest temperature (300 °C). This reaction prevented the exploration of higher temperatures, but the similar evolution of arsenious and arsenic speciation with temperature up to 300 °C suggests that this speciation would prevail at higher temperatures as well.

4.2. Molecular interactions

From a physical-chemical perspective, As^{III} and As^{V} can be compared in terms of chemical bonding. Our studies on arsenic (Pokrovski *et al.*, 2002a; Testemale *et al.*, 2004; this study) demonstrate that covalent entities such as $As^{III}(OH)_3$ or $As^{V}O(OH)_3$ are very little sensitive to the modification of the solvent, as indicated by the constancy of the As-O distance with temperature and the very weak increase of the MSRD disorder parameter at the investigated temperatures $T < 300$ °C. It would be interesting to explore higher temperatures and check whether the tetrahedral AsO_4 entity is modified by the strong and dynamic modifications within the solvent intermolecular structure (weaker H-bonding, heterogeneities, etc.) characteristic of the supercritical regime, and at the critical isochore more specifically. It was the case for the AsO_3 entity where an opening of the pyramidal structure was proposed by Testemale *et al.* (2004), but its structure offers less screening between As atoms and the solvent molecules than in the more compact tetrahedral AsO_4. Nevertheless, the similitude between two species and their covalent nature suggest a similar behaviour at high temperatures. In particular, like $As(OH)_3$ (Pokrovski *et al.*, 2002a), $AsO(OH)_3$ is expected to persist in low-density fluids (<0.3 g.cm^{-3}) of low dielectric constant that favours neutral species stability (Pokrovski *et al.*, 2005b).

The need for a molecular description of the transport processes in fluids is at the interface between two fields: geochemistry (where the speciation is needed) and physics of condensed matter (where the nature of inter- and intramolecular interactions is explored). Thus, the input from molecular dynamics and energetics computational methods, which are widely used in physical chemistry of condensed matter, is expected to be very useful in geochemical topics. It would provide a molecular description of the solvation processes and help interpret spectroscopic data (Raman, XAS). A good example in the case of As is given by computational work of Tossell (1997) and Myneni *et al.* (1998). Interestingly, both our experimental results from XANES simulations and their conclusions from theoretical simulations converge, in particular regarding the distortion of the $As^{V}O_4$ tetrahedron.

Acknowledgements: The authors acknowledge the European Synchrotron Radiation Facility for provision of synchrotron radiation beamtime and facilities, and thank the BM32-IF and BM30-FAME staff for their assistance.

References

Baes, C.F., Jr. & Mesmer, R.E. (1976): The hydrolysis of cations. Wiley Inter-science, New York.

Baur, W.H. & Kahn, A.A. (1970): On the crystal chemistry of salt hydrates. VI. The crystal structures of disodium hydrogen orthoarsenate heptahydrate and of disodium hydrogen orthophosphate heptahydrate. *Acta Cryst.*, **26**, 1584–1596.

Booth, C.H. & Bridges, F. (2005): Improved self-absorption correction for fluorescence measurements of extended x-ray absorption fine-structure. *Phys. Scr.*, T**115**, 202–204.

Borisova, A.Y., Pokrovski, G.S., Pichavant, M., Freydier, R., Candaudap, F. (2010): Arsenic enrichment in hydrous peraluminous melts: insights from femtosecond laser ablation-inductively coupled plasma – quadrupole mass spectrometry, and in situ X-ray absorption fine structure spectroscopy. *Am. Mineral.*, **95**, 1095–1104.

Brugger, J., Etschmann, B., Liu, W., Testemale, D., Hazemann, J.-L., Emerich, H., van Beek, W., Proux, O. (2007): An XAS study of the structure and thermodynamics of Cu(I) chloride complexes in brines up to high temperature (400°C, 600 bar). *Geochim. Cosmochim. Acta*, **71**, 4920–4941.

Bunker, G. (1983): Application of the ratio method of EXAFS analysis to disordered systems. *Nucl. Instrum. Methods Phys. Res.*, **207**, 437–444.

Charnock, J.M., Polya, D.A., Gault, A.G., Wogelius, R.A. (2007): Direct EXAFS evidence for incorporation of As^{5+} in the tetrahedral site of natural andraditic garnet. *Am. Mineral.*, **92**, 1856–1861.

D'Angelo, P., Roscioni, O.M., Chillemi, G., Della Longa, S., Benfatto, M. (2006): Detection of second hydration shells in ionic solutions by XANES: computed spectra for Ni^{2+} in water based on molecular dynamics. *J. Am. Chem. Soc.*, **128**, 1853–1858.

Gout, R., Pokrovski, G.S., Schott, J., Zwick, A.A. (1997): Raman spectroscopy study of arsenic speciation in aqueous solution to 275°C. *J. Raman Spectrosc.*, **28**, 725–730.

Hattori, K., Takahashi, Y., Guillot, S., Johanson, B. (2005): Occurrence of arsenic (V) in forearc mantle serpentinites based on X-ray absorption spectroscopy study. *Geochim. Cosmochim. Acta*, **69**, 5585–5596.

James-Smith, J., Cauzid, J., Testemale, D., Liu, W., Hazemann, J.-L., Proux, O., Etschmann, B., Philippot, P., Banks, D., Williams, P., Brugger, J. (2010): Arsenic speciation in fluid inclusions from gold deposits using microbeam X-ray absorption spectroscopy from ambient to homogenisation temperatures. *Am. Mineral.*, **95**, 921–932.

Joly, Y. (2001): X-ray absorption near-edge structure calculations beyond the muffin-tin approximation. *Phys. Rev. B*, **63**, 125120.

Kelly, S.D., Hesterberg, D., Ravel, B. (2008): Analysis of soils and minerals using x-ray absorption spectroscopy. *in* ''Methods of soil analysis, Part 5, mineralogical methods'', A.L. Ulery & L.R. Drees, eds. Soil. Sci. Soc. Am., Madison, WI, 387–464.

Krause, M.O. & Oliver, J.H. (1979): Natural widths of atomic K and L levels, K alpha X-ray lines and several KLL Auger lines. *J. Phys. Chem. Ref. Data*, **8**, 329–338.

Loehr, T.M. & Plane, R.A. (1968): Raman spectra and structures of arsenious acid and arsenites in aqueous solution. *Inorg. Chem.*, **7**, 1708–1714.

Mustre de Leon, J., Rehr, J.J., Zabinsky, S.I., Albers, R.C. (1991): Ab initio curved-wave x-ray-absorption fine structure. *Phys. Rev. B*, **44**, 4146–4156.

Myneni, S.C.B., Traina, S.J., Waychunas, G.A., Logan, T.J. (1998): Experimental and theoretical vibrational spectroscopic evaluation of arsenate coordination in aqueous solutions, solids, and at mineral-water-interfaces. *Geochim. Cosmochim. Acta*, **62**, 3285–3300.

Nordstrom, D.K. & Archer, D.G. (2003): Arsenic thermodynamic data and environmental geochemistry. *in* ''Arsenic in ground water'', A.H. Welch & K.G. Stollenwerk, eds. Kluwer Academic Publishers, 1–25.

Oelkers, E.H., Benezeth, P., Pokrovski, G.S. (2009): Thermodynamic databases for water-rock interaction. *in* ''Thermodynamics and kinetics of water-rock interactions'', E.H. Oelkers & J. Schott, eds. Mineral. Soc. Am. Geochem. Soc., *Rev. Mineral. Geochem. Ser.*, **70**, 1–46.

Perfetti, E., Pokrovski, G.S., Ballerat-Busserolles, K., Majer, V., Gibert, F. (2008): Densities and heat capacities of aqueous arsenious and arsenic acid solutions to 350°C and 300 bar, and revised thermodynamic properties of $As(OH)_3$(aq), $AsO(OH)_3$(aq) and iron sulfarsenide minerals. *Geochim. Cosmochim. Acta*, **72**, 713–731.

Pertlik, F. (1978): Structure refinement of cubic As_2O_3 (arsenolithe) with single crystal data. *Czech. J. Phys.*, **28**, 170–176.

Pokrovski, G.S. & Sanchez-Valle, C. (2010): Arsenic fate in subduction-zone fluids: insights from in-situ X-ray absorption spectroscopy in the diamond anvil cell. *Journal of Conference Abstracts*, EMPG-XIII, Toulouse, France, 12–14 April.

Pokrovski, G.S., Gout, R., Zotov, A.V., Schott, J., Harrichoury, J.-C. (1996): Thermodynamic properties and stoichiometry of the arsenic(III) hydroxide complexes at hydrothermal conditions. *Geochim. Cosmochim. Acta*, **60**, 737–749.

Pokrovski, G.S., Bény, J.-M., Zotov, A.V. (1999): Solubility and Raman spectroscopic study of As^{III} speciation in organic compound-water solutions. A hydration approach for aqueous arsenic in complex solutions. *J. Solution Chem.*, **28**, 1307–1327.

Pokrovski, G.S., Zakirov, I.V., Roux, J., Testemale, D., Hazemann, J.-L., Bychkov, A.Y., Golikova, G.V. (2002a): Experimental study of arsenic speciation in vapor phase to 500°C: implications for As transport and fractionation in low-density crustal fluids and volcanic gases. *Geochim. Cosmochim. Acta*, **66**, 3453–3480.

Pokrovski, G.S., Kara, S., Roux, J. (2002b): Stability and solubility of arsenopyrite, FeAsS, in crustal fluids. *Geochim. Cosmochim. Acta*, **66**, 2361–2378.

Pokrovski, G.S., Roux, J., Hazemann, J.-L., Testemale, D. (2005a): An X-ray absorption spectroscopy study of argutite solubility and germanium aqueous speciation in hydrothermal fluids to 500°C and 400 bar. *Chem. Geol.*, **217**, 127–145.

Pokrovski, G.S., Roux, J., Harrichoury, J.C. (2005b): Fluid density control on vapor-liquid partitioning of metals in hydrothermal systems. *Geology*, **33**, 657–660.

Ramirez-Solis, A., Mukopadhyay, R., Rosen, B.P., Stemmler, T.L. (2004): Experimental and theoretical characterization of arsenite in water: insights into the coordination environment of As-O. *Inorg. Chem.*, **43**, 2954–2959.

Ravel, B. & Newville, M. (2005): ATHENA, ARTEMIS, HEPHAESTUS: data analysis for x-ray absorption spectroscopy using IFEFFIT. *J. Synchrotron Radiat.*, **12**, 537–541.

Shock, E.L., Sassani, D.C., Willis, M., Sverjensky, D.A. (1997): Inorganic species in geological fluids: correlations among standart molal thermodynamic properties of aqueous ions and hydroxide complexes. *Geochim. Cosmochim. Acta*, **61**, 907–950.

Soldo, Y., Hazemann, J.-L., Aberdam, D., Inui, M., Tamura, K., Raoux, D., Pernot, E., Jal, J.-F., Dupuy-Philon, J. (1998): Semiconductor-to-metal transition in fluid selenium at high pressure and high temperature: an investigation using X-ray absorption spectroscopy. *Phys. Rev. B*, **57**, 258–268.

Tamura, K., Inui, M., Hosokawa, S. (1995): XAFS measurements at high temperatures and pressures. *Rev. Sci. Instrum.*, **66**, 1382–1384.

Testemale, D., Hazemann, J.-L., Pokrovski, G.S., Roux, J., Joly, Y., Argoud, R., Geaymond, O. (2004): Structural and electronic evolution of the As(OH)3 molecule in high-temperature aqueous solutions: an x-ray absorption investigation. *J. Chem. Phys.*, **121**, 8973–8982.

Testemale, D., Brugger, J., Liu, W., Etschmann, B., Hazemann, J.-L. (2009): In-situ X-ray absorption study of iron(II) speciation in brines up to supercritical conditions. *Chem. Geol.*, **264**, 295–310.

Tossell, J.A. (1997): Theoretical studies on arsenic oxide and hydroxide species in minerals and in aqueous solution. *Geochim. Cosmochim. Acta*, **61**, 1613–1623.

Vaughan, D.J. (2006): Arsenic. *Elements*, **2**, 71–75.

Received 3 November 2010
Modified version received 4 February 2011
Accepted 2 March 2011